Transient Load Share Management of a Diesel Electric Hybrid

Sotirios K. Topaloglou

Laboratory of Marine Engineering (LME),
National Technical University of Athens,
s.topaloglou@gmail.com

George Papalambrou

Laboratory of Marine Engineering (LME),
National Technical University of Athens,
george.papalambrou@lme.ntua.gr

Konstantinos Bardis

Laboratory of Marine Engineering (LME),
National Technical University of Athens,
kwstasbardis@gmail.com

Nikolaos Kyrtatos

Laboratory of Marine Engineering (LME),
National Technical University of Athens,
nkyrt@lme.ntua.gr

September 11, 2017

Abstract

In this paper, a transient load share methodology for a hybrid diesel electric marine propulsion system is presented. Aim of the system is the performance enhancement and reduction of gaseous emissions during low-load transient operation. The controlled variable is λ while the manipulated variable is the torque from the electric motor regulated by a frequency inverter.

The model for the λ behavior is based on experimental identification while λ values in feedback loop come from an actual and a virtual sensor, the later based on first principles modeling. A nominal model is used for the synthesis of a robust H_∞ controller for the controlled variable regulation.

Experimental results in a full scale hybrid diesel electric powertrain under realistic loading scenarios verified the successful hybridization.

I. Introduction

In view of the ever tightening emission requirements for port operations imposed by the legislation authorities on sea-going vessels, novel technologies in the field of marine propulsion have to be implemented. One promising technology for emission reduction and fuel efficiency enhancement is the hybrid diesel-electric propulsion.

Typically in the existing marine technology framework, ships are equipped with direct-driven propulsion machinery occasionally combined with a shaft generator system, known as Power Take Out (PTO), generating power for some of the electrical demands of ship. Current trends consider the usage of auxiliary power to assist the main engine in some load situations, such as high bollard pull, sailing in icy conditions, harbor maneuvering or "take-home" power, thus reverting the role to Power Take In (PTI) operation through powertrain *hybridization*. In this way, the size of main engine could be optimized to the propulsion power needed under normal conditions while additional power boost can be taken from auxiliary generators as required. For relevant info see [1].

Depending on their architecture, Hybrid Electric Powertrains (HEP) fall into one of several categories: 1) parallel; 2) series; or 3) power split. In the parallel scheme, both the engine and the motor are connected to the transmission, and thus, they can power the vehicle either separately or in combination. In series hybrids, the electric motor (EM) is the only means of providing the demanded power. Finally, the power split scheme can operate either as a parallel or a series HEP, combining the advantages of both but with increased complexity.

The performance of a hybrid powertrain in terms of reducing both fuel consumption and exhaust emissions critically depends on the energy management strategy (EMS). An EMS is the supervising control algorithm that determines how the total power demand is shared between the power sources [2]. One main category of EMSs with limited, however, potential for marine power plants due to the requirement of the exact knowledge of the driving cycle include the optimization techniques found in [3], [4], [5] and [6]. Moreover, heuristic methods such as fuzzy logic and neural networks have been adopted in [7], [8] and [9] but neither achieve an optimal solution not robustness with respect to performance.

The above control strategies have dealt mainly with fuel economy without a particular emphasis in emission reduction. The subject of emission reduction in a quasi-static framework is discussed in [10], [2], [11] and [12]. However the incorporated quasi-static models for emission formation disregard the substantial rise of pollutant emissions during transient operation of diesel engines (DE) due to the presence of thermodynamic delays mainly associated with turbocharger [13].

The formulation of transient emission reduction is presented in [14], where the optimal EMS for a diesel hybrid electric powertrain is calculated, considering the transient pollutant particulate matter emissions. In the same direction, [15], an EMS is considered using a frequency-domain power distribution (FDPD) strategy, which requires a priori knowledge of the loading profile.

The reduction of NOx emission in both steady state and transient operating conditions has been examined in [16]. The optimal power split in steady state is provided by an EMS while the reduction of transient NOx emissions is achieved through the smoothing of the DE torque demand by utilizing the EM torque as torque compensator. However, the dynamic control law is not robust with respect to exogenous disturbance and unmodeled dynamics that inevitably exist in real-world hybrid electric powertrains.

In this paper, a model-based controller is presented, which tracks the air ratio of an Internal Combustion Engine (ICE), while engaging an electric motor, in a hybrid propulsion arrangement. The controller does not interfere with the fueling of the ICE, which allows their application also as a retro-fit solution. For the λ measurement a physical commercial sensor and a virtual sensor

design were used. The λ virtual sensor exhibited a performance which was matching that of the commercial physical sensor, and at some instances was even better, due to the smaller response time it offered.

λ number is defined as the ratio of the actual to the stoichiometric air-to-fuel ratio (AFR) (AFR/AFR_{st}).

The rationale behind our approach is to reduce the intensity of the transient loading phenomenon in the DE with the aid of the EM. It takes advantage of the rapid conversion between electrical and mechanical energy in EM to assist the DE that has a limited torque delivery due to its thermodynamic nature. The concept of the above methodology is presented schematically in Fig. 1, in the typical marine propulsion operation. The electric motor assists the diesel engine at low-load operation, where the internal combustion engine produces low torque, so as to meet up with the torque demand faster. With this setup the initially small margin (i.e. the available torque that the propulsion system has available for acceleration during transient operation) can be significantly increased.

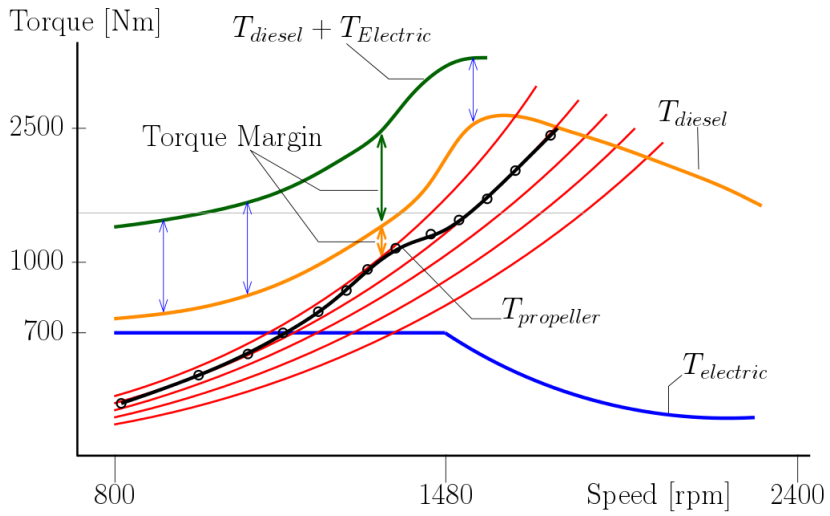

Figure 1: Schematic of load acceptance in the Hybrid Integrated Propulsion Powertrain.

While closed loop control of emissions in DEs has been an active research field for more than fifteen years [17], this paper aims to present a novel marine application, where λ-manipulation is achieved only with the additional degree of freedom stemming from the hybridization of the powertrain.

In the standard λ setup, the control is performed through the fuel injection system; in our case the factory fueling commands are not overridden but by applying torque from the electric motor, the torque from diesel is directly affected so that λ is implicitly regulated.

λ number is defined as the ratio of the actual to the stoichiometric air-to-fuel ratio (AFR) (AFR/AFR_{st}).

The λ in the cylinder is controlled by regulating the λ measured in the exhaust after the combustion takes place and the travel of exhaust gas through the manifold reaches λ sensor.

The reasons for choosing λ in the proposed control method are twofold: it is a good indicator of particulate matter (PM) emissions, which are directly associated with black smoke (exhaust gas opacity) and it directly relates to the combustion temperature which relates to NOx. In addition, a λ "virtual sensor" is implemented and tested in closed loop, offering the benefit of

direct estimation of λ in the cylinder where combustion takes place.

Regarding a possible fully electric layout for ship propulsion, a series hybrid configuration could be considered. In this case, there would be only one electric transmission path between the ICE and the ship propeller. An energy storage system of high turnaround efficiency would also be required [18]. The ICE would operate at constant speed, with little transient loading. In such a configuration, a controller that aims at assisting the ICE during transient loading, like the one presented in this paper, would be of limited usability.

The paper is structured as follows: In Sec. II the hybrid diesel-electric test bed is described. The plant model is derived experimentally in Sec. III while the design of the λ virtual sensor is described in Sec. IV. An H_∞ controller is synthesized in Sec. V and its validity is experimentally examined in Sec. VI. The last section provides the conclusions.

II. Testing Facility Description

The hybrid propulsion powertrain test bed (seen in Fig. 2) consists of an ICE in parallel connection to an electric machine. As such, the rotational speeds of ICE and EM are identical, whereas the supplied torques add together. The desired torque demand is applied through a water brake, which is manipulated by a separate H_∞ controller developed in-house.

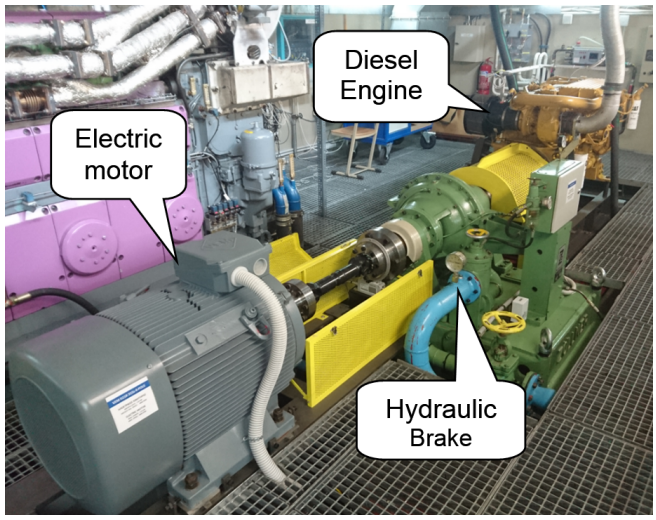

Figure 2: The hybrid electric test bed.

The prime mover is a production-type, CATERPILLAR 3176B 6-cyl. 10-liter marine diesel engine, with a rated power output of 425 kW at 2300 rpm. The ICE is coupled to an EM which is a standard 3-phase asynchronous induction motor, with a rated power of 112 kW. The EM is connected to a frequency inverter unit, enabling the torque output regulation of the EM at a predefined rotational speed. Finally, the water brake has a load capacity of 1200 kW, with maximum speed at 4000 rpm.

Measurements present in the test bed include: NOx/oxygen (Continental Uninox 24V), exhaust gas opacity (AVL 439), fuel mass flow (ABB CoriolisMaster FCM2000), turbocharger speed (μ epsilon), torque and speed (HBM), intake manifold pressure. A schematic representation of the installed sensors and engine parameters is given in Fig. 3.

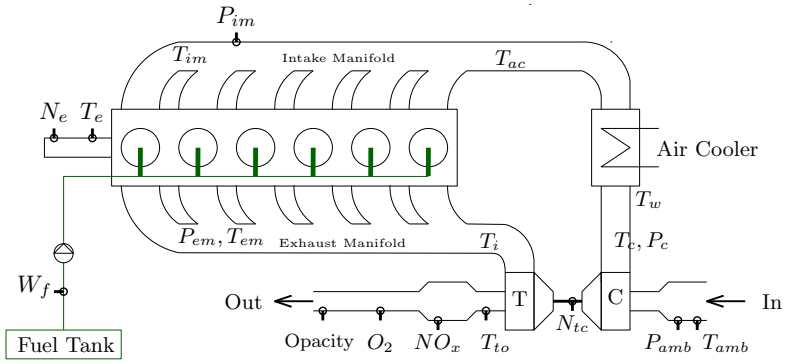

Figure 3: Installed sensors (in circle) and engine parameters in experimental diesel engine.

The whole test bed is controlled and monitored in real time by a dSpace DS1103 controller board, programmed under the Matlab/Simulink environment.

III. Model Identification

A fundamental step in the problem of λ closed loop control is the derivation of a control-oriented model of the plant.

The traditional approach towards the problem of AFR estimation is through phenomenological Mean Value Models of the individual engine components, e.g. the intake and exhaust manifolds, the turbocharger, the cylinders etc; for more information see [19].

Linear identification methods were the preferable option for the problem in consideration, due to the lack of efficiently detailed information about the engine components. Various models were obtained around an appropriate engine operating point. Linear control-oriented models for AFR dynamics in SI engines based on identification have been used successfully in the past; see [20] and [21].

The method employed to measure input and output data for system identification was to apply a Pseudo-Random Binary Signal (PRBS) at the frequency inverter of the electric motor as torque command (FrInvCmd), and to measure the resulting λ values of the diesel engine; thus $[u; y] = [FrInvCmd; \lambda]$. The identification experiment was carried out with constant torque demand at T_d= 500 Nm, as imposed by the water brake, and constant shaft speed N_e= 1600 rpm. Data was collected with a rate of 1 kHz, low-pass filtered and divided in two sets, one for identification and one for validation.

The choice of input signal was made based on its implementation simplicity, white-noise-like autocorrelation function, suitability for linear system identification and control over the shaping of its spectrum ([22], [23]). The magnitude of the PRBS signal was chosen so that the crest factor obtains its maximum value with consideration of the physical limitations of the system while the order of 9-bits was selected so that the dominant frequencies of the identified system were covered.

The identification of the transfer function was carried out with the Matlab/System Identification Toolbox, [24] and command **tfest**, where calculated model parameters are updated using the recursive prediction error method. Further details regarding the identified model can be found in Appendix A.

In order to verify the accuracy of the identified model, the output of the nominal model was compared to the output of actual λ values from time series data, as shown in Fig. 4.

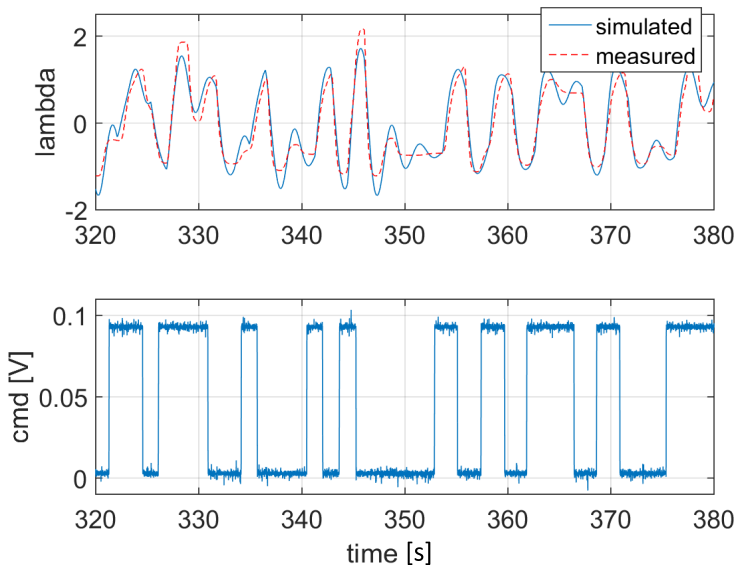

Figure 4: Simulated and measured λ (top); The input PRBS signal.

The H_∞ controller design requires a linear, finite dimensional system model. For this purpose, the time delay was replaced with a 20-th order Padé element, adopting the approach where for delays up to 40 ms a first order approximation is chosen, and for every additional 40 ms, one order is added ([25]).

IV. Virtual Lambda Sensor

At the hybrid propulsion powertrain, the physical sensor for λ is installed in the exhaust duct of the diesel engine, 1 m after the turbine outlet, which introduces an additional delay to that of the sensor itself (approx. 120 ms). Also, during fast load reductions, the Engine Control Unit (ECU) senses the acceleration and drastically reduces the injected fuel or even stops fueling, causing large spikes in the measurement of λ. When such signal is fed to the controller, the command will display undesirable oscillatory behavior.

In order to eliminate such problems, a *virtual* λ sensor was derived and used in the control loop. The main parts of the virtual sensor model consist of the fuel path, the air path and the gas mixing, as shown in the block diagram of Fig. 5. The virtual lambda sensor model makes use of the physical variables which are available through measurements, namely the rotational speed of the engine N_e, the turbocharger speed N_{tc}, the pressure at the air cooler inlet p_{im} and through map (look-up table) like the torque T_e produced by ICE.

i. Fuel Path Model

The engine is approximated as a Willans machine [26], where the engine is assumed to be an energy converter which converts the available fuel chemical energy W_{in} into output flow $\phi_{out} = \omega_e$ and effort variables $\epsilon_{out} = T_e$. Although the energy conversion is non-linear, an affine relationship between the input power and the output effort variables is a fair approximation for a specified engine speed.

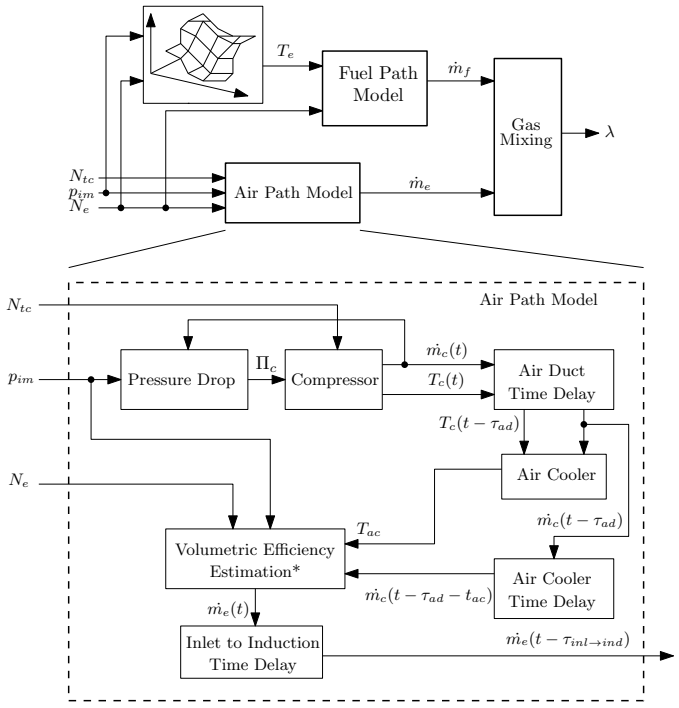

Figure 5: Virtual sensor model fundamental components.

For each time instant, the following equation holds

$$T_e = \frac{e(\omega_e) \cdot \dot{m}_f \cdot H_{LV}}{\omega_e} - T_{loss}(\omega_e) \tag{1}$$

where ω_e is the engine speed in rad/s, H_{LV} is the lowest calorific value of the fuel and e is the thermodynamic efficiency of the thermodynamic cycle.

The injected fuel will affect the torque output of the engine only after the injection to power cycle (PC) [19]. For this reason, a time delay is introduced into Eq. 1 which is transformed to

$$T_e(t) = \frac{e \cdot \dot{m}_f(t - \tau_{inj\to PC})}{\omega_e(t)} \cdot H_{LV} - T_{loss} \tag{2}$$

Equation 2 can be written as

$$\dot{m}_f(t) = \frac{\omega_e(t + \tau_{inj\to PC}) \cdot (T_e(t + \tau_{inj\to PC}) + T_{loss})}{H_{LV} \cdot e} \tag{3}$$

so that the unknown output is the fuel flow.

The final estimation of λ could be improved if the fuel injected in the ICE could be known from the ECU parameters, instead of the above calculations for m_f.

ii. Air Path Model

The air path model is composed of blocks which calculate the volumetric efficiency, the pressure drop in compressor and air cooler, the compressor performance, the conditions in the outlet of air

cooler as well as the time delays of air through the air duct, the air cooler and induction in the cylinders. At this part of the model, the conversion from crank-angle to time also takes place.

The output of this model is the air mass flow aspirated by the engine, $\dot{m}_e$, while the inputs are the engine speed N_e, the turbocharger speed N_{tc} and the pressure at the air cooler inlet p_{im}.

Detailed information for the modeling can be found in Appendix. B.

iii. In-cylinder Gas Mixing

At each time instant, the value of λ for the fresh charge mixture of air and fuel is given by

$$\lambda = \frac{AFR}{AFR_{st}} = \frac{\dot{m}_e/\dot{m}_f}{AFR_{st}} \tag{4}$$

However, a part of the exhaust gases remains inside the cylinder and is mixed with the fresh air charge. The final value of $\lambda(t)$ would be a weighted average of $\lambda(t - \tau_{ieg})$ which is the value of λ for the previous cycle and of $\lambda_{fc}(t)$ which is the value of λ for the new air that is aspirated inside the cylinder. The derived relationship is

$$\lambda(t) = \frac{\lambda(t - \tau_{ieg}) \cdot m_{res}(t) + \lambda_{fc}(t) \cdot [m_e(t) + m_f(t)]}{m_e(t) + m_f(t) + m_{res}(t)} \tag{5}$$

where the masses that appear in the equation above can be computed from the corresponding mass flows using the integration formula

$$m(t) = \dot{m}(t - \tau_{ieg}) \cdot \tau_{ieg} \tag{6}$$

The interval of integration is the time between the induction and the exhaust cycle

$$\tau_{ieg} = \frac{2\pi \cdot 2}{\omega_e \cdot z} \tag{7}$$

iv. Validation

In order to verify the accuracy of the virtual λ values, the output of the model was compared to actual (measured) λ values, as shown in Fig. 6. Since no other chemical process takes place between the combustion in the cylinder and the measurement point of the installed oxygen sensor, we consider the measured lambda value in the exhaust path to be equal to the lambda value in the cylinder. During load application, estimated λ values show good tracking behavior; when load is removed a higher λ value can be observed.

V. Control Synthesis

The robust controller for λ closed loop control is obtained as an H_∞ mixed sensitivity controller. Interested reader is referred to [27] for the theoretical aspects of the H_∞ controller synthesis algorithm. Mixed sensitivity H_∞ controllers have been implemented successfully in diverse diesel engine applications, see for example [28].

The H_∞ mixed sensitivity is suitable when dealing with modelling uncertainties since they can be compensated in the specifications of the complementary sensitivity T weight. In addition to the sensitivity S and the complementary sensitivity T, the transfer KS from r to u is incorporated in the scheme to restrict the size and the behavior of the input signals.

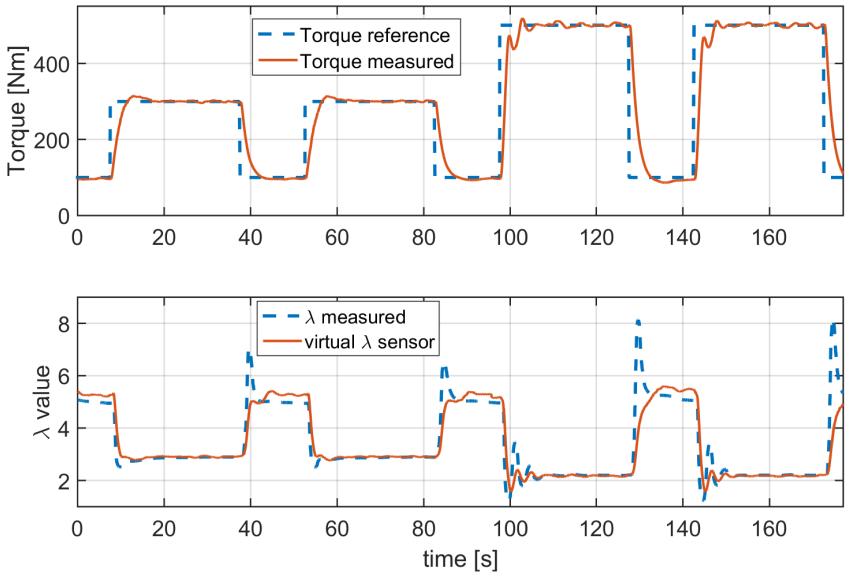

Figure 6: λ comparison between estimated and measured values. Top plot shows the applied load. changed line style

Following the determination of the closed loop response weights, the controller derivation can be formulated as a solution to a minimization problem. In this stage, a stabilizing controller K is obtained, so that the H_∞ norm of the extended plant transfer function T_{zw} between the exogenous inputs to the system (d, r, n) and the exogenous outputs (z_1, z_2, z_3), where r is the reference signal, d are the disturbances, n is the noise signal, e is the error and u is the control output, is minimized as in Eq. 8.

$$\|T_{zw}\|_\infty = \left\| \begin{bmatrix} W_P S \\ W_U K S \\ W_T T \end{bmatrix} \right\|_\infty \leq \gamma \tag{8}$$

Typically $\gamma = 1$ so that the closed loop transfer functions are limited by the inverse of the weighting functions W_i over the whole frequency range.

The weights W_P, W_T and W_U that determine the frequency response of S, T and K are chosen as in Eqs. 9-11, as can be found in [29].

$$W_P(s) = \frac{s/M_P + \omega^\star_{BP}}{s + \omega^\star_{BP} \cdot A_P} \tag{9}$$

$$W_T(s) = \frac{s + \omega^\star_{BT}/A_T}{s \cdot M_T + \omega^\star_{BT}} \tag{10}$$

$$W_U(s) = \frac{s + \omega^\star_{BU}/A_U}{s \cdot M_U + \omega^\star_{BU}} \tag{11}$$

where the parameters A_i and M_i correspond to the asymptotic behavior of the weighting functions W_i for $s \to 0$ and $s \to \infty$, respectively. The frequency $\omega^\star_B$ is approximately the bandwidth requirement.

At steady state it is desirable that the plant output closely follows the reference command and the controller rejects the exogenous disturbances.

At steady state it is desirable that the plant output closely follows the reference command and the controller rejects the exogenous disturbances. For this reason $A_T \simeq 1$ and A_P is chosen as small as possible. Integral action with a value of A_P=0 is avoided due to the numerical instabilities in the H_∞ synthesis algorithm. The requirements for small overshoot and robustness with respect to uncertainty is lumped into the condition of small weighting parameter W_P. Furthermore, the selected bandwidths $\omega^\star_{BT}$ and $\omega^\star_{BP}$ have to compromise the conflicting requirements of fast rise time and low noise sensitivity. The controller weight W_U is specified in such way so as to allow tight control at low frequencies and noise attenuation at high; the physical limitations of the system are also taken into account. Weight W_T is chosen so that complementary sensitivity T is limited to avoid unnecessarily high bandwidth of the control system. Various cases were examined in order to evaluate controller performance and robustness (model order, dead times, un-modelled dynamics, disturbances).

The H_∞ controller was designed using graphical programming, in the Matlab/Simulink environment. The controller is then compiled in C++ language using the built-in functions, and then downloaded to the real-time dSpace platform.

The Bode diagram of the frequency response of S, KS and T as well as the inverse of the selected weights $W_i^{-1}(s)$ is given in Fig. 7.

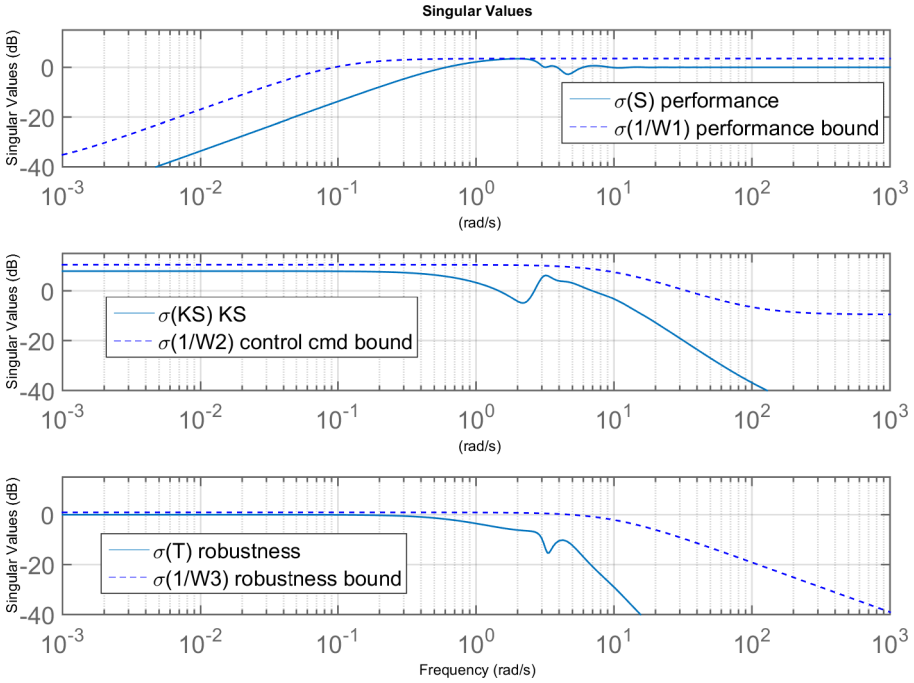

Figure 7: Bode diagrams of S/KS/T.

The controller was implemented in discrete state-space form, with sampling time of 1 ms, in Simulink.

The block diagram for the closed loop system is presented in Fig. 8. The controller utilizes the measured λ values and a reference value, which depending on the mode of operation, is either a constant (static ref.) or is derived from look-up tables. The main sensors for feedback control are the oxygen sensor (Smart NOx), the engine speed sensor and the inlet manifold pressure (MAP). Alternatively, with the availability of virtual λ sensor, the λ measurement is replaced by

λ calculations in closed loop. The resulting controller command is the input to the frequency inverter of the EM.

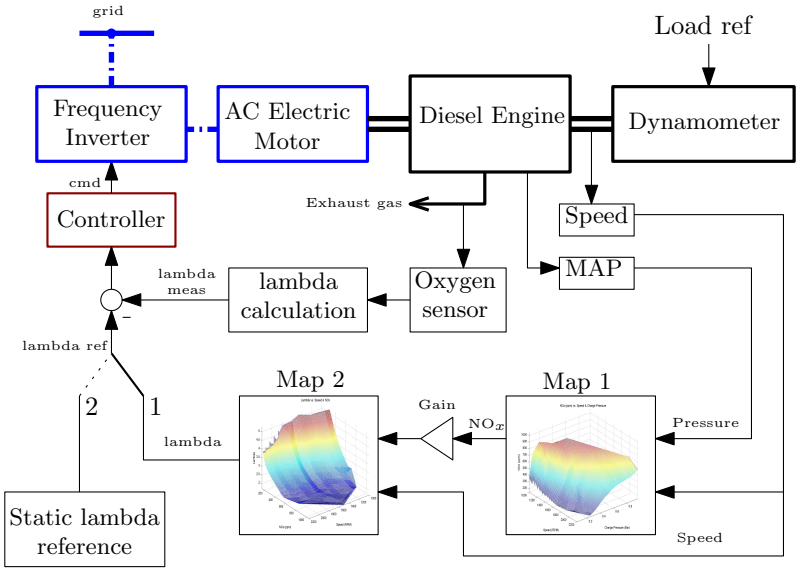

Figure 8: The closed loop system with sensors and map references.

VI. Experimental Results

Various experiments were conducted on the hybrid propulsion powertrain, in order to evaluate the performance of the load share strategy.

These are divided in two main sections, as follows. The first set of experiments resembles a generator on-board a ship, where the engine operates at constant speed (1600 rpm) and with alternating load. In this case the controller receives a static lambda reference value. In the second set of experiments the engine simulates a propeller loading operation, with alternating speed and torque. In this case a set of look-up tables for the λ reference points was used. In both loading scenarios, the performance is assessed when the controller receives λ feedback from the physical sensor or the virtual one.

i. Generator mode

An experiment with load steps from approx. 100-300 Nm and 100-500 Nm, at 1600 rpm, is shown in Fig. 9. The static λ reference was set at $\lambda_{ref} = 3$, after repetitive experiments of the same loading cycle. As can be seen in the second subplot, the purpose of the proposed controller is to track the imposed λ setpoint by engaging the EM. The output of the hybrid controller can be seen in the third subplot of the same figure. The use of the virtual sensor in the control loop gives less oscillatory command and the EM reaches its maximum torque faster than the hybrid setup with the physical sensor. Also, the proposed controller provides good tracking performance during changes in the load, for both cases of feedback.

The λ set point represents the only parameter needed for tuning the strategy for a specific loading profile. As soon as there is a rising edge in the applied total torque, the measured λ drops almost instantly, creating an error between the measured and static λ values. The controller uses

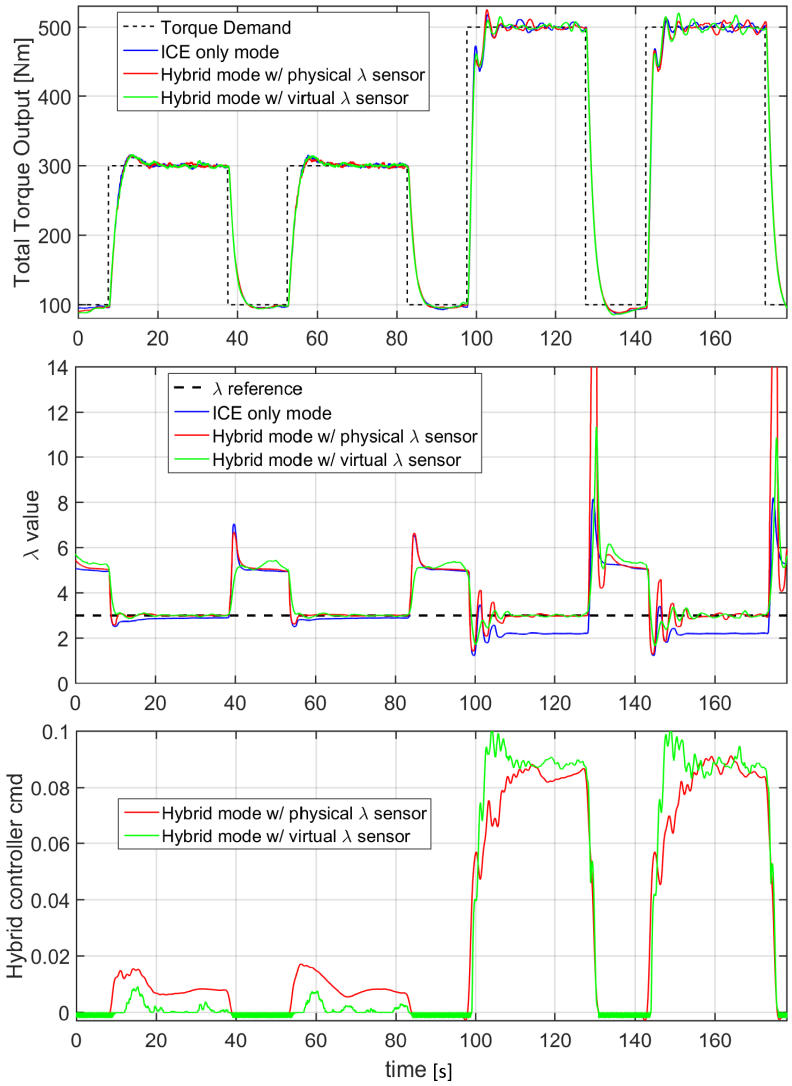

Figure 9: Effect of the hybrid powertrain on λ value during generator mode with static reference point.

this error as input and engages the EM, producing torque. It can be observed that the proposed controller provides good tracking performance during the load change and at steady state. To avoid any performance deterioration in case of the inverter command saturation, all integrators are implemented with anti-reset-windup. The hybrid setup with the virtual sensor provides slightly faster command output to the electric motor, compared to the physical sensor, due to the delays of the installed λ sensor.

In Fig. 10, the impact of the hybrid powertrain on the produced NO_x and exhaust gas opacity, as compared to the conventional setup can be noted. The total torque demand is still met, but the electric motor assists the ICE while it is accelerating, in order to reduce exhaust opacity, NO_x content and fuel consumption (although not shown here). Both sensor setups show almost the same behavior. It is shown that during acceleration, the produced exhaust gas opacity values are

significantly lower, around 25%. The NO_x content is slightly decreased during the first moments of the load change (first "spike"), but is greatly reduced once the EM engages and contributes to the total load demand.

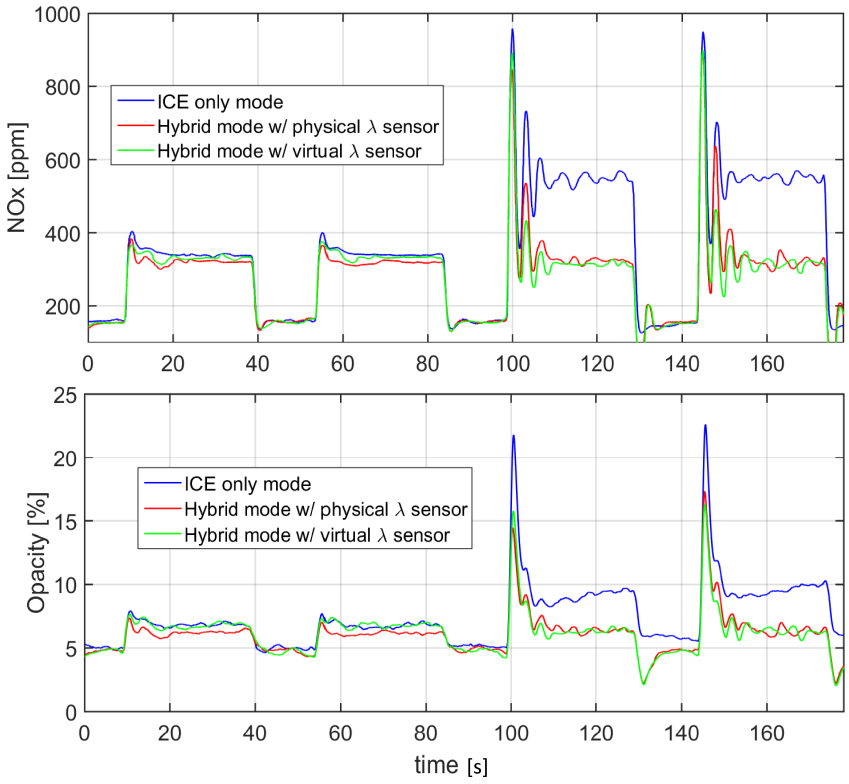

Figure 10: Effect of the hybrid powertrain on NO_x and exhaust gas opacity, during generator mode with static reference point.

ii. Propeller mode

There is a common relation between the torque (power) and speed in ship propulsion, known as the *propeller law* [30]. It is known that shaft rotational speed (n_p) is almost linearly proportional to the ship's speed (V_s)

$$n_p = c_1 \cdot V_s \tag{12}$$

The power required to tow the ship at ship speed V_s with resistance R, is the effective (towing) power P_E (eq. 13). Using the assumed proportionality of resistance and ship speed squared, effective speed is, as a first approximation, proportional to the cube of speed V_s.

$$P_E = R \cdot V_s \tag{13}$$

$$P_E = c_2 \cdot V_s^3 \tag{14}$$

For a ship equipped with a fixed pitch propeller, the necessary power requirement, P, is proportional to shaft speed, n, to the power of three (propeller law), by combining equations 12-14

as in

$$P = c\, n^3 \tag{15}$$

where c is a constant number. In our case, $c_3 = 1.56 \cdot 10^{-4}$, which was derived from the on-board measurements and utilized for the experimental propeller curve.

In order to assess the proposed power split methodology against realistic data from ships, appropriate measurement equipment was installed on-board a high-speed vessel with waterjets, so as to gather actual engine performance and emissions data during normal service. The voyage included high speed cruising, port approaching at low speed and maneuvering, idling for unloading and loading of the vessel and immediate departure afterwards, as shown in Fig. 11.

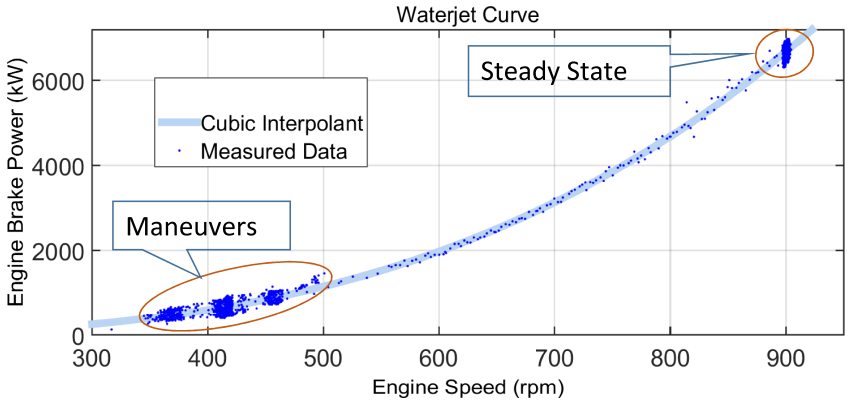

Figure 11: Measured propeller power demand curve from on-board data.

This data was utilized as reference for the design and evaluation of loading profiles during experiments, as in Fig. 12. The torque changes from approx. 120 Nm to 700 Nm and the engine speed from 1100 rpm to 1850 rpm.

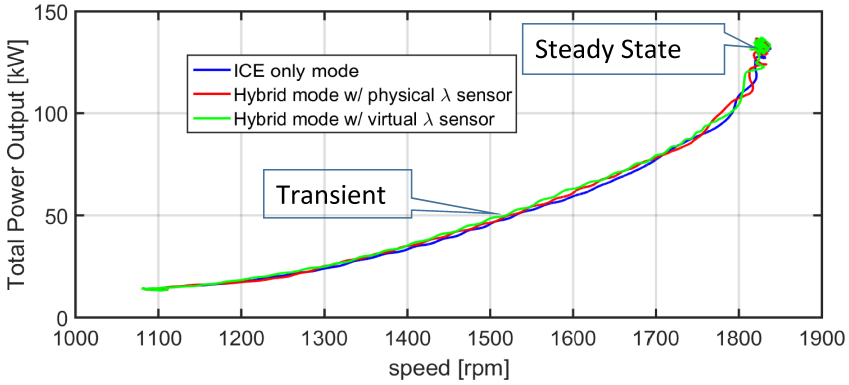

Figure 12: Propeller power curve on test bed.

The λ set point for these experiments is derived from a set of two static maps, with the independent variables N_e and P_{inlet}, as seen in Fig. 8. The output of the first map (Map 1) is the expected NO_x value for any given engine speed and inlet manifold pressure. This NO_x value is then multiplied by the desired NO_x reduction percentage (in the form of a gain) and used as input for the second map (Map 2), which in turn gives the λ set point (reference) value. The gain values

used in this work come after trial end error, but on-going work with optimization will provide appropriate numbers. The two maps are created from experimental data collected from the hybrid propulsion powertrain, under steady state operation (see Fig. 13).

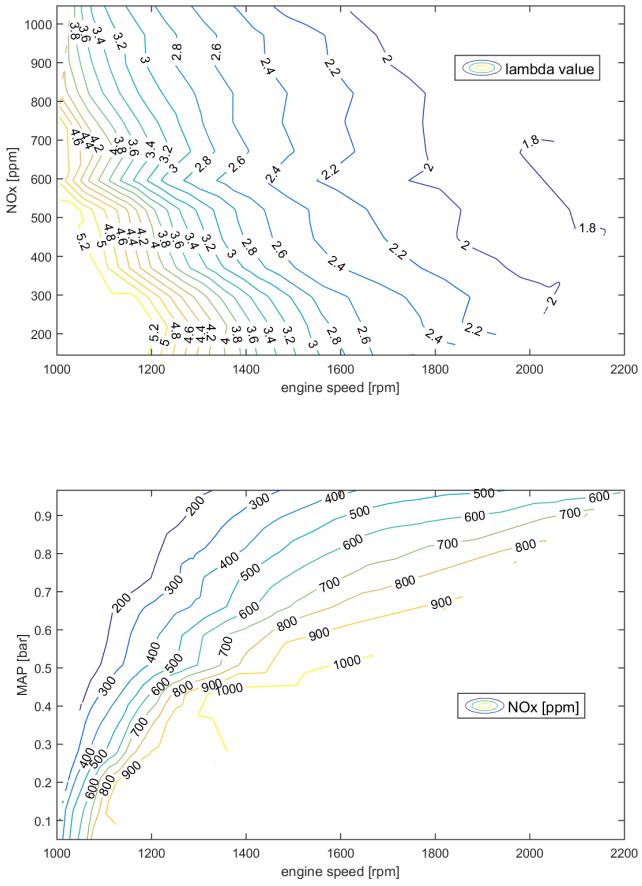

Figure 13: Reference maps for λ based on NOx, engine speed (top) and for NOx based on MAP, engine speed.

The main idea of dynamic λ reference points is to shift the ICE engine at more efficient operating points only during transient loading, where the measured λ drops rapidly, by engaging the EM. The EM command is imposed by a positive error between the reference λ value and the measured one, while in steady state condition, the error minimizes and thus the EM switches off. The designed controller leads to sensible reduction of NO_x emissions, exhaust gas opacity and fuel consumption (not shown), with respect to the conventional (non-hybrid) powertrain, during acceleration. The electric power consumption is not taken into account, as this work focuses only on the transient loading phenomena. Also, further studies have shown that in general more than 50% of total diesel engines pollutant emissions can be attributed to transient effects [[14]].

The corresponding λ values, controller command and the resulting EM torque are depicted in Fig. 14. The recorded λ values are higher using the hybrid setup (leaner combustion) than using the conventional one (i.e. without EM assistance), as the controller tracks the reference λ values imposed by the look-up tables. As the virtual sensor is based on the air path of the engine, which is faster than the exhaust path used by real sensor, the virtual λ value drops faster than the

physical one, thus creating a bigger error when compared to the reference λ value. In turn, this leads to faster engagement of the EM by the controller.
Fig. 15 shows the measured gas emissions of NO_x and exhaust gas opacity. For the NO_x emissions of the hybrid setup with the physical sensor, a reduction of 16% was recorded during acceleration, while the use of the virtual sensor saved another 5%. The measured opacity was about 20% less during transient loading for both sensor setups, when compared to the conventional powertrain. In steady state operation, the dynamic λ setpoints as imposed by the look-up tables, and the measured/virtual λ values converge, and the EM switches off.

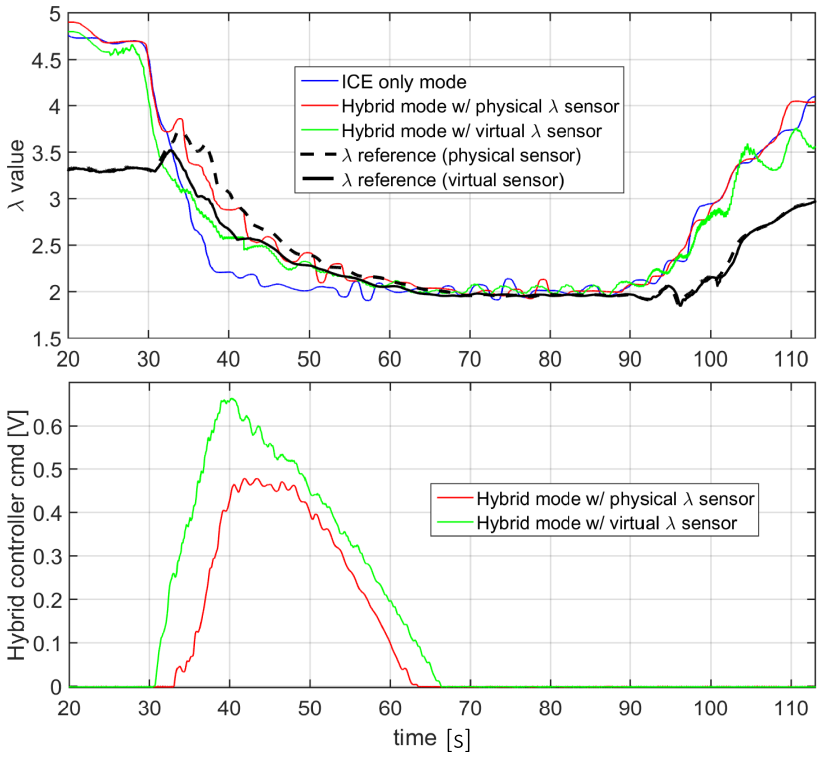

Figure 14: Effect of the hybrid powertrain on lambda during a propeller loading curve.changed line style

VII. Conclusions

In this work, a power management controller for a diesel electric parallel hybrid powertrain was investigated, where both a commercial λ sensor and a virtual one provided feedback. Two sets of experiments were conducted on the hybrid propulsion powertrain. The first set of experiments used a static λ reference value and the engine operating at constant speed and with alternating load, which corresponds to a generator on- board a ship. In the second set of experiments the engine was operated with changing speed and torque, simulating a propeller. The proposed controller provided good tracking performance, both with static reference points and with dynamic ones, as imposed by the created look-up tables. It was shown that the integration of feedback of lambda of a diesel engine in a marine hybrid setup, during acceleration, via controlling the electric motor, can lead to improved performance and lower exhaust gas emissions that are attributed to

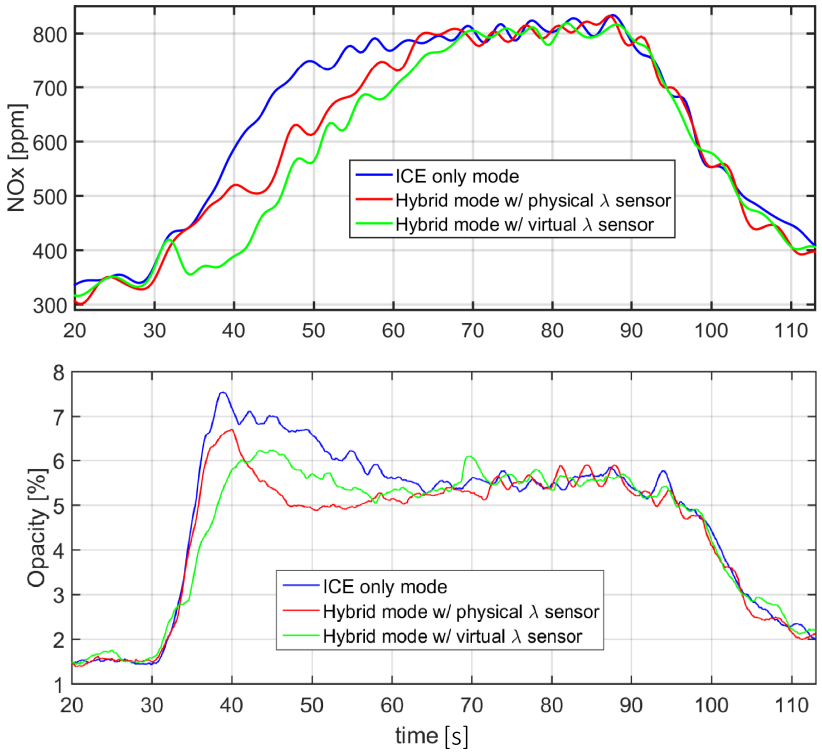

Figure 15: Effect of the hybrid powertrain on NOx and exhaust gas opacity during a propeller loading curve.

transient effects. The virtual sensor provided equal performance with the commercial one, and at some instances even better, due to the smaller response time it offers.

In the proposed solution, the controller did not interfere with the ICE fueling parameters, thus providing capability for an individual retro-fit solution.

Current on-going work will provide the optimal set points to the λ controller, taking into consideration parameters like fuel consumption, NOx and smoke opacity emissions as well as the available amount of torque from electric motor.

VIII. Acknowledgments

The authors gratefully acknowledge the support of EC/DG RTD H2020/HERCULES-2 project, as well as the support of Lloyds Register Foundation, within the LRF NTUA Centre of Excellence in Ship Total Energy-Emissions-Economy, for the development and extension work on the hybrid integrated propulsion powertrain and related HIPPO-1 diesel electric test bed, described in this paper. This project has also received funding from the European Union's Horizon 2020 research and innovation programme under grant agreement No 634135. The doctoral studies of author S.T. are supported through a DNV-NTUA sponsor agreement, which is gratefully acknowledged.

Appendix A

The identified transfer function G with input the command to the frequency inverter, $u = FrInvCmd$; and output $y = \lambda$ is presented in Eq. 16. The operating point used for the model identification was 1600 rpm for engine speed and 500 Nm for applied load. Delay is in s.

$$G = \frac{e^{-0.79s}(16.1s^4 + 134.2s^3 + 376s^2 + 1455s + 1628)}{s^5 + 4s^4 + 25.4s^3 + 50.4s^2 + 108.7s + 101.3} \tag{16}$$

Appendix B

This section provides details about the air path model, with blocks which calculate the volumetric efficiency, the pressure drop in compressor and air cooler, the compressor performance, the conditions in the outlet of air cooler as well as the time delays of air through the air duct, the air cooler and inlet.

Volumetric Efficiency Estimation

Engine is modeled as a volumetric pump with the aspirated mass of air into the engine given by

$$\dot{m}_e = \frac{\eta_v V_{cyl} p_{im} z N_e}{R T_{im} 120} \tag{17}$$

where V_{cyl} is the cylinder volume, N_e is the speed of engine in rpm, η_v is the volumetric efficiency and z is the number of cylinders.

According to [31], the volumetric efficiency depends on engine speed N_e and a time-varying parameter $\theta(t)$ that needs to be identified. Under this assumption, Eq. 18 is derived.

$$\eta_v = P(N_e(t)) \cdot \theta(t) \tag{18}$$

Pressure Drop

The compression pressure ratio can be evaluated from

$$\Pi_c = \frac{p_{im} + \zeta_{total} \frac{1}{2} \rho_3 c_3^2 + \Delta p_{ac}}{p_{amb}} \tag{19}$$

where Δp_{ac} is the pressure drop in the air cooler, c_3 is the average flow velocity at the compressor outlet and ζ_{total} is a coefficient which incorporates the main pressure losses occur in the pipeline.

Compressor

Incoming gas enters the impeller eye with velocity

$$c_1 = \frac{\dot{m}_c}{\rho_1 \cdot A_1} \tag{20}$$

where ρ_1 is the density at the compressor inlet.

At the outlet of the impeller the radial component of the velocity is given by

$$c_{2r} = \frac{\dot{m}_c}{\rho_2 \cdot \pi \cdot D_2 \cdot t_2} \tag{21}$$

and the tangential velocity can be calculated as follows

$$c_{2t} = \sigma \cdot (U_2 - c_{2r} cot(\beta_2)) \tag{22}$$

where U_2 is the impeller tip velocity and σ is the so called "slip factor".

The isentropic efficiency $\eta_{is,c}$ is corrected, so as to take into account other types of losses that are difficult to model analytically. Such type of losses are the clearance losses, the back flow losses and the volute losses. The corrected isentropic efficiency is given by

$$\eta_{is,c} = \frac{\Delta h_{ideal}}{\Delta h_{ideal} + \Delta h_{loss}} - \Delta\eta_c - \Delta\eta_{bf} - \Delta\eta_v \tag{23}$$

The overall pressure rise in compressor is given by

$$\frac{p_{03}}{p_{01}} = (\frac{T_{03is}}{T_{01}})^{\frac{\gamma}{\gamma-1}} \tag{24}$$

The air in the engine room is assumed to be at temperature T_{amb} and pressure p_{amb}. When the air enters the compressor, as a result of the velocity increase, the temperature drops from T_{amb} to T_1 as follows

$$T_1 = T_{amb} - \frac{1}{2} c_1^2 \tag{25}$$

The static pressure at the compressor inlet is given by

$$p_1 = p_{1s} - \zeta_c \frac{1}{2} \rho_{01} c_1 \tag{26}$$

where

$$p_{1s} = p_{amb} \cdot (\frac{T_1}{T_{amb}})^{\frac{\gamma}{\gamma-1}} \tag{27}$$

is the pressure drop for an isentropic expansion and ζ_c is a friction coefficient. Additionally, estimating the density at the compressor inlet from the ideal gas law we can compute the dynamic pressure at compressor inlet as follows

$$p_{01} = p_1 + \frac{1}{2} \rho_1 c_1^2 \tag{28}$$

The dynamic pressure at the compressor outlet is estimated with the following formula

$$p_{03} = p_3 + \frac{1}{2} \rho_3 c_3^2 = \Pi_c \cdot p_{amb} + \frac{1}{2} \rho_3 c_3^2 \tag{29}$$

Air Cooler

The temperature immediately after the compressor can be calculated from the compression ratio Π_c and the known isentropic efficiency $\eta_{is,c}$. The temperature is given by

$$T_c = T_{amb} \cdot ((\Pi_c)^{(\gamma-1)/\gamma} - 1)/\eta_{is,c} + 1) \tag{30}$$

The air cooler is modeled as a heat exchanger; its effectiveness is assumed to be a quadratic function of the air flow $\dot{m}_c$, as in

$$\epsilon = 1 - c \cdot {\dot{m}_c}^2 \tag{31}$$

The air temperature T_i in the cooler outlet is given by

$$T_{ac} = \epsilon \cdot T_w + (1 - \epsilon) \cdot T_c \tag{32}$$

Intake Manifold

Intake manifold is modeled as a fixed volume with homogeneous thermodynamic variables [19]. The mass balance yields

$$\frac{dm_{im}}{dt} = \dot{m}_c - \dot{m}_e \tag{33}$$

where $\dot{m}_c$ is the mass delivered from the compressor, $\dot{m}_e$ is the mass aspirated by the engine and $\frac{dm_{im}}{dt}$ is the rate of change in the intake manifold mass of air accumulation.

The implementation of the virtual λ as well as the adaptation law and the proof of parameter convergence can be found in [31].

Delays Computation

Air from the compressor is delivered through the air pipe to the air cooler and the time needed for the fluid to travel along the pipe can be calculated by

$$\tau_{ad} = \frac{L_{ad}}{c_3} \tag{34}$$

Similarly, the time delay due to the presence of the air cooler is

$$\tau_{ac} = \frac{L_{ac} \cdot A_{ac} \cdot \rho_{av}}{\dot{m}_c} \tag{35}$$

where ρ_{av} is the mean density between the inlet and outlet of the air cooler $\rho_{av} = \frac{1}{2} \cdot (\rho_{ac^+} + \rho_3)$.

The inlet-to-induction delay can be computed as

$$\tau_{inl \to ind} = \frac{3/2}{\omega_e \cdot z} \tag{36}$$

The air in the intake manifold will only enter the engine during the intake stroke of one of the cylinders. For an engine with z number of cylinders the induction stroke is repeated approximately every $(360^o + 180^o)/z$ of the crank shaft angle.

References

[1] E. Boletis. Integration of propulsion system from the point of view of efficiency optimization. *In Proceedings of the 28th CIMAC World Congress 2016, Helsinki, Finland*, 2016.

[2] C. Lin, H. Peng, J. W. Grizzle, and J. Kang. Power management strategy for a parallel hybrid electric truck. *IEEE Transactions on Control Systems Technology*, 11(6):839–849, 2003.

[3] A. Sciarretta and L. Guzzella. Control of hybrid electric vehicles. *IEEE Control Systems Magazine*, pages 60–70, April 2007.

[4] M. Ramsbottom and F. Assadian. Use of approximate dynamic programming for the control of a mild hybrid. In *Proceedings of WMG Hybrid Conference*, December 2006.

[5] C. C. Lin, J. M. Kang, J. W. Grizzle, and H. Peng. Energy management strategy for parallel hybrid electric truck. In *Proceedings of the American Control Conference*, pages 2878–2883, 2001.

[6] G. Ripaccioli, A. Bemporad, F. Assadian, C. Dextreit, S. Di Cairano, and I. Kolmanovsky. Hybrid modeling, identification, and predictive control: An application to hybrid electric vehicle energy management. In *Hybrid Systems: Computation and Control*, volume 5469, pages 321–335. Springer-Verlag, 2009.

[7] M. Salman, N. J. Schouten, and N. A. Kheir. Control strategies for parallel hybrid vehicles. *Proceedings of the American Control Conference*, 1:524–528, 2000.

[8] N. Schouten, M. Salman, and N. Kheir. Fuzzy logic control for parallel hybrid vehicles. *IEEE Transactions on Control Systems Technology*, 10:460–468, 2002.

[9] B. M. Baumann, G. N. Washington, B. C. Glenn, and G. Rizzoni. Mechatronic design and control of hybrid electric vehicles. *IEEE/ASME Trans. on Mechatronics*, 5:58–72, 2000.

[10] E. D. Tate, J. W. Grizzle, and H. Peng. SP-SDP for fuel consumption and tailpipe emissions minimization in an evt hybrid. *IEEE Transactions on Control Systems Technology*, 18(3):673–687, 2010.

[11] C. Lin, H. Peng, and J. W. Grizzle. A stochastic control strategy for hybrid electric vehicles. *Proceedings of American Control Conference*, (5):4710–4715, 2004.

[12] V. H. Johnson, K. Wipke, and D. Rausen. Hev control strategy for real-time optimization of fuel economy and emissions. *SAE 2000 Transactions Journal of Engines*, 109(2000-01-1543), 2000.

[13] C. Rakopoulos and E. Giakoumis. Review of thermodynamic diesel engine simulations under transient operating conditions. *SAE 2006 Transactions Journal of Engines*, (2006-01-0884), 2006.

[14] T. Nuesch, M. Wang, P. Isenegger, C. H. Onder, R. Steiner, and L. Guzella. Optimal energy management for a diesel hybrid electric vehicle considering transient pm and quasi-static nox emissions. *Control Engineering Practice*, 29:266–276, 2014.

[15] Y. Kim, A. Salvi, J. Siegel, Z. Filipi, A. Stefanopoulou, and T. Ersal. Hardware-in-the-loop validation of a power management strategy for hybrid powertrains. *Control Engineering Practice*, 29, 2014.

[16] O. Grondin and L. Thibaultand C. Qurel. Transient torque control of a diesel hybrid powertrain for NOx limitation. In *Proceedings of the 2012 IFAC Workshop on Engine and Powertrain Control, Simulation and Modeling*, volume 3, pages 286–295, 2012.

[17] A. Amstutz and L. K. Del Re. Ego sensor based robust output control of egr in diesel engines. *IEEE Transactions on Control Systems Technology*, 3(1):413–420, 1995.

[18] J. M. Miller. Propulsion systems for hybrid vehicles. *The Institution of Engineering and Technology*, 2008.

[19] L. Guzzella and C. Onder. *Introduction to Modeling and Control of Internal Combustion Engine Systems*. Springer, London, 2nd edition, 2004.

[20] R. De Filippi and R. Scattolini. Idle speed control of a F1 racing engine. *Control Engineering Practice*, 14:251–257, 2006.

[21] S. Hashimoto, H. Okuda, Y. Okada, S. Adachi, S. Niwa, and M. Kajitani. An engine control systems design for low emission vehicles by generalized predictive control based on identified model. In *Proceedings of the IEEE International Conference on Control Applications*, pages 2411–2416, 2006.

[22] T. Poloni, T. A. Johansen, and B. Rohal'-Ilkiv. Modeling of air-fuel ratio dynamics of gasoline combustion engine with arx network. *Journal of Dynamic Systems, Measurement, and Control*, 130(6), 2008.

[23] L. Ljung. *System Identification, Theory for the User*. Prentice Hall, Upper Saddle River, NJ, 2nd edition, 1999.

[24] L. Ljung. *System Identification Toolbox*, September 2015.

[25] C. Roduner, C. Onder, and H. Geering. Automated design of an air/fuel controller for an si engine considering the three-way catalytic converter in the $h\infty$ approach(1997). *In Proceedings of the fifth IEEE Mediterranean Conference on Control and Systems, Paphos, Cyprus*, 1997.

[26] G. Rizzoni, L. Guzzella, and B. Baumann. Unified modeling of hybrid electric vehicle drivetrains. *IEEE/ASME Transactions on Mechatronics*, 4:246–257, September 1999.

[27] J. C. Doyle, K. Glover, P. P. Khargonekar, and B. A. Francis. State-space solutions to standard H_2 and H_∞ control problems. 34(8):831–847, August 1989.

[28] E. Alfieri, A. Amstutz, and L. Guzzella. Gain-scheduled model-based feedback control of the air/fuel ratio in diesel engines. *Control Engineering Practice*, 17(12):1417–1425, December 2009.

[29] S. Skogestad and I. Postlethwaite. Multivariable feedback control analysis and deisgn. *John Wiley and Sons*, 2005.

[30] H.K. Woud and D. Stapersma. Design of propulsion and electric power generation systems. *The Institue of Marine Engineering, Science and Technology*, 2003.

[31] O. Storset, A. Stefanopoulou, and R. Smith. Adaptive air charge estimation for turbocharged diesel engines without exhaust gas recirculation. *IEEE/ASME Journal of Dynamic Systems, Measurement, and Control*, 126, 2003.